Studies of an orthorhombic Jahn-Teller system: Cr^{3+} in GaAs by EPR

1990 J. Phys.: Condens. Matter 2 2841

(http://iopscience.iop.org/0953-8984/2/12/007)

J. Phys.: Condens. Matter **2** (1990) 2841–2856. Printed in the UK

Studies of an orthorhombic Jahn–Teller system: Cr^{3+} in GaAs by EPR

L W Parker†§‖, C A Bates†, J L Dunn†, A Vasson‡ and A-M Vasson‡

† Physics Department, The University, Nottingham NG7 2RD, UK

‡ LPMC, Physique 4 (URA CNRS No 796), Université Blaise Pascal-Clermont-Ferrand II, 63177-Aubière, France

Received 6 November 1989

Abstract. Results from isofrequency and frequency-dependent thermally detected EPR experiments on the GaAs:Cr^{3+} system are reported. These data and those obtained previously by Krebs and Stauss using conventional EPR are then used to obtain the parameters appearing in the effective Hamiltonian of the $^4T_1$ ground state of the Cr^{3+} ion. It is shown that this effective Hamiltonian is that of a strongly coupled, orthorhombic Jahn–Teller system in which certain random static strains play an important rôle in determining the experimental results. It is suggested that the GaAs:Cr^{3+} system is an ideal example of an orthorhombic Jahn–Teller system as seen by EPR because the first excited ^2E state of the ion is very close in energy to the $^4T_1$ ground state. This causes much admixing, so the resonances within the two lowest Kramers doublets are clearly separated. The difficulties in deducing values for all the fundamental parameters are also discussed.

1. Introduction

GaAs:Cr^{3+} is probably the best known example of a strongly coupled, orthorhombic Jahn–Teller system. However, studies of this system are complicated because the Cr^{3+} ion has a weak electron paramagnetic resonance (EPR) spectrum whose observability decreases rapidly at temperatures above 5 K and is also much affected by sample mounting. In addition, it is very difficult to detect the Cr^{3+} ion by optical techniques.

Work on chromium-doped GaAs began in earnest in the 1970s in a search for semi-insulating substrates for devices. Although the technological interest in this system is diminishing, a basic physical understanding of it is far from complete. For these reasons, a comprehensive set of thermally detected (TD) EPR experiments has been carried out in our laboratories in order to provide further data on the GaAs:Cr^{3+} system. These new data will be used together with the original EPR data of Krebs and Stauss (1977a, to be referred to as KS) and of Stauss and Krebs (1980, to be referred to as SK) to present a detailed theoretical model for this unique JT system. This will involve the derivation of and fitting to an effective Hamiltonian that describes the ground states of the system. It is possible to do this now that calculations of the second-order reduction factors for all

§ Now at: GPT, Technology Drive, Beeston, Nottingham NG9 1LA, UK.

‖ Reprint requests to Professor C A Bates or Dr J L Dunn.

0953-8984/90/122841 + 16 $03.50

three idealised orbital triplet Jahn–Teller systems have just been completed (Bates and Dunn 1989, Dunn and Bates 1989b).

2. Experimental data

2.1. Summary of published experimental data

The Cr^{3+} ion in GaAs was first identified by KS using EPR. Later SK reported the effects of uniaxial stress on their EPR spectra. In these experiments it was very clear that the absolute and relative signal amplitudes were dependent upon the internal strains introduced during the initial mounting of the sample and subsequent cooling.

No optical absorption related to Cr^{3+} has been reported although Deveaud *et al* (1984) have followed the earlier suggestion of Koschel *et al* (1976) that the zero-phonon line (ZPL) at 0.66 eV associated with the 0.57 eV luminescence band is due to a transition to the $^4T_1(^4F)$ ground state of Cr^{3+}. Recently, Dunn and Bates (1987) have suggested that the expected $^4T_1$–$^4T_2$ transition could be absent because the two triplets are subject to different-symmetry JT effects, and so the oscillator parts of the associated JT vibronic states have very little overlap due to their separation in phonon-coordinate space. This suggestion is given quantitative support by the theoretical calculations of Bacci *et al* (1989) using the angular overlap model.

In contrast, the Cr^{3+} ion strongly scatters phonons. Benkovskis *et al* (1981) attributed some low frequency acoustic relaxation effects to Cr^{3+}. Other phonon scattering experiments by Challis *et al* (1982) and Ramdane *et al* (1983), using thermal conductivity measurements, and by Hamdache *et al* (1983), using tunnel junction phonon spectroscopy techniques, show probable scattering of phonons from Cr^{3+} ions at a frequency $\simeq$700 GHz. The remaining scattering observed at lower frequencies in both types of phonon experiment referred to above is not expected to be due to isolated Cr^{3+} ions but to either Cr^{3+}–V_{As} centres (Austen *et al* 1984) or to Cr^{3+}–Cr^{3+} pairs (Challis *et al* 1989). (V_{As} signifies a vacancy at an As site.)

The experimental results (EPR, the absence of a ZPL and the strong phonon scattering) clearly indicate that the Cr^{3+} ions in GaAs are very strongly coupled to the lattice and that the $^4T_1$ ground state is subject to a very strong orthorhombic JT effect. Also, the experimental conditions under which the EPR spectra are observed in GaAs clearly indicate that strain-stabilised resonances (Dunn *et al* 1986, Bates and Stevens 1986, Dunn and Bates 1989b) dominate the spectra.

2.2. TD EPR experiments

The technique of TD EPR, which is particularly sensitive to strongly coupled ions, has been used to obtain further information on the GaAs:Cr^{3+} system using many crystals of chromium-doped GaAs from different sources. Our first measurements on chromium-doped GaAs, using a fixed frequency ν of 9.3 GHz, were described by Rezki *et al* (1982) and relate to the isolated substitutional Cr^{3+} ion. Both the availability of higher, variable magnetic fields B (up to 3T), and the possibility of placing the sample in the waveguide and varying ν, have enabled us to obtain much more information from our TD EPR spectrometer than was obtained in the original EPR experiments of KS and SK (see, for example, the discussion in Bates *et al* (1988) for the GaAs:Cr^{2+} system).

Four of the crystals we have studied contain Cr^{3+} as identified initially from the similarity of the isofrequency curves with those found originally by KS. These crystals

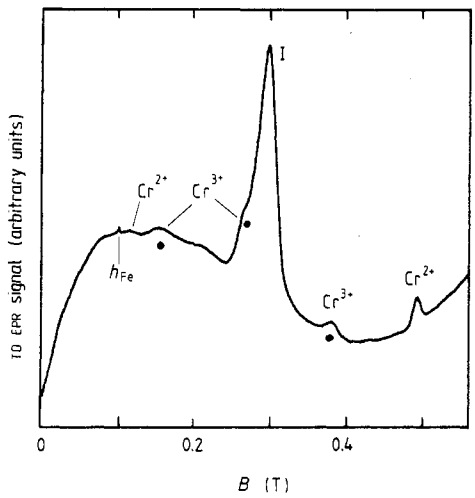

Figure 1. A typical TD EPR spectrum showing the Cr^{3+} (●) and Cr^{2+} resonances in GaAs (sample RTC 399-752) at 8.7 GHz with the static magnetic field $\boldsymbol{B}$ along the [110] axis. The h_{Fe} resonance is due to Fe^{2+} ions in very low concentrations in the alumina holder. The sample and the holder are together responsible for the resonance I.

come from a variety of sources; two from RTC, France, one from the Plessey Co., UK, and one from the SNP works, Ziarnad Hronom, Czechoslovakia. All samples were semi-insulating at liquid helium temperatures, so the necessary condition for clear signals in TD EPR experiments with our current experimental procedures was met. The RTC samples were sufficiently large to allow both magnetic ($\boldsymbol{B}_{rf}$) and electric ($\boldsymbol{E}_{rf}$) field transitions to be observed simultaneously.

Measurements were carried out at liquid helium temperatures with $\boldsymbol{B}$ rotated in the $(1\bar{1}0)$ and (001) planes. The frequency ν was varied between 8.0 and 12.4 GHz and the samples were fixed at different positions and in different orientations within the guide. Figure 1 gives typical spectra, figures 2 and 3 show isofrequency curves for two different orientations of the sample and figure 4 shows curves obtained for the resonant field $\boldsymbol{B}_{res}$ as ν was varied with $\boldsymbol{B}$ along the $[1\bar{1}0]$ and [110] axes. The results displayed in figures 1–4 were all obtained from the RTC sample 512-904 for which the Cr^{3+} resonances were more intense than those obtained from the other samples. Note that Cr^{2+} ions were present in these samples together with other unknown defects as indicated in figure 1. However, for clarity only the resonances that are subsequently associated with isofrequency curves of the Cr^{3+} ion are shown in figures 2–4. The samples were not externally stressed; it was assumed that cooling the sample after mounting generated sufficient internal stresses to enable the spectra to become visible. The relative strengths of the resonances varied with the sample used, the positioning of it in the waveguide and with the relative directions of $\boldsymbol{B}$, $\boldsymbol{B}_{rf}$ and $\boldsymbol{E}_{rf}$. However, the values of $\boldsymbol{B}_{res}$ were the same for all samples with the same geometry and same ν. We suppose therefore that the spectra are characteristic of the same ion, namely a substitutional Cr^{3+} ion on a Ga site. The experiments of Krebs and Stauss (1977a, b) demonstrated that the Cr^{3+} ion can be converted to an isolated substitutional Cr^{2+} ion under suitable illumination, by a reversible process.

3. Theoretical background

The original work of KS showed clearly that the Cr^{3+} ions seen by EPR were at sites of orthorhombic symmetry. It was assumed that the tetrahedral crystal field splits the free

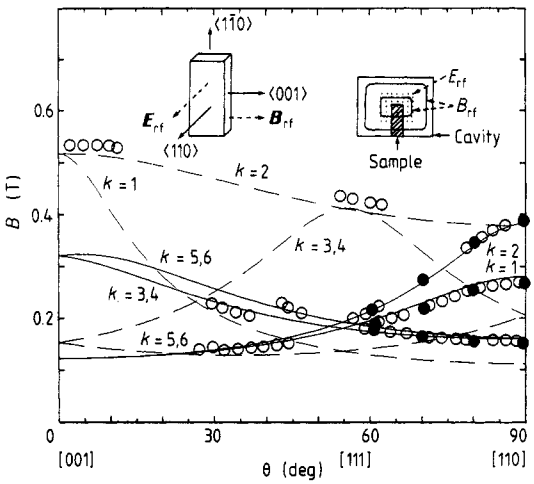

Figure 2. The calculated isofrequency curves and TD EPR data for Cr^{3+} ions with $\boldsymbol{B}$ in the $(1\bar{1}0)$ plane with $\nu = 8.7$ GHz. (Note that some of the experimental points at high fields near to the [001] and [111] directions are not necessarily from the Cr^{3+} centre.) The points indicated thus ● were included in the fitting routine.

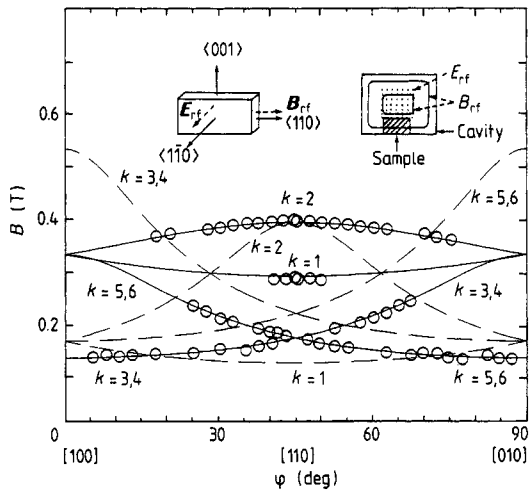

Figure 3. The calculated isofrequency curves and TD EPR data for Cr^{3+} ions with $\boldsymbol{B}$ in the (001) plane with $\nu = 8.83$ GHz.

ion term ^4F into a $^4T_1$ ground state, which is split further by an orthorhombic field into three orbital singlets, each with a spin degeneracy of 4. The lowest of these singlets was described by the spin Hamiltonian ($S = \frac{3}{2}$)

$$\mathcal{H}_s = \mu_B \sum_i g_i B_i S_i + D[S_Z^2 - \tfrac{1}{3}S(S+1)] + E(S_X^2 - S_Y^2) \tag{3.1}$$

where X, Y, Z are appropriate orthorhombic axes. The eigenstates of $\mathcal{H}_s$ consist of two doublets separated by an energy $2Q$ ($=2(D^2 + 3E^2)^{1/2}$). Alternatively the ground and

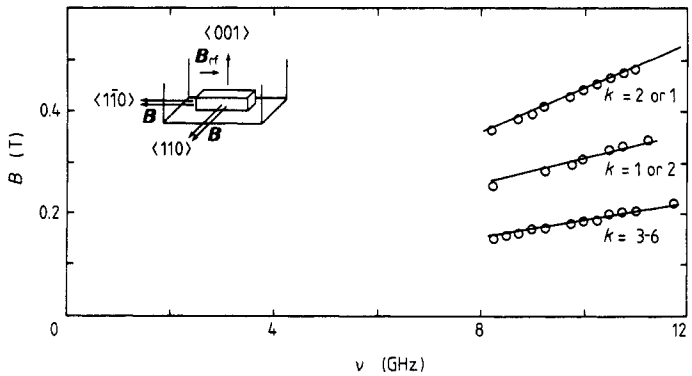

Figure 4. The frequency-dependent TD EPR measurements for Cr^{3+} ions. The experimental points were obtained with $\boldsymbol{B}$ along [1$\bar{1}$0] and [110]. The calculated theoretical results are also shown by full lines and are labelled by the appropriate site label k.

excited state doublets may each be described by an effective $S' = \frac{1}{2}$ and a $\mathbf{g}$ tensor by the simple Hamiltonian

$$\mathcal{H}_s' = \mu_B \boldsymbol{B} \cdot \mathbf{g} \cdot \boldsymbol{S}' \tag{3.2}$$

provided that the microwave quantum is much smaller than $2Q$. The EPR isofrequency curves were fitted by taking

$$g_X' = 2.367 \qquad g_Y' = 1.636 \qquad g_Z' = 5.154$$

in $\mathcal{H}_s'$ or, in terms of the parameters of $\mathcal{H}_s$ by

$$E/D = 0.263 \qquad g_X = 1.962 \qquad g_Y = 1.985 \qquad g_Z = 2.002.$$

The splitting $2Q$ was estimated to be $5\,cm^{-1}$. A higher value of $10.4 \pm 1.5\,cm^{-1}$ was obtained for $2Q$ from a study of population effects. (Note that KS reported that the precision quoted in their earlier work (SK) was over-optimistic.) The EPR spectrum was described initially in terms of a large static, orthorhombic JT distortion. In the second paper, this statement was amended as a result of a series of experiments under controlled uniaxial stresses (SK). It was shown that it was possible to induce a dynamic-to-static JT transition and that the minima involved were orthorhombic.

4. Theory of deep level impurities

In order to obtain further physical insight into the nature of the $^4T_1$ ground states of the Cr^{3+} ion in GaAs, it is necesary to derive an effective Hamiltonian to describe the spin–orbit coupling, the Zeeman terms and the strain. This will be carried out in two stages; the first stage is to use a one-electron model to describe the ion and the second stage is to incorporate the strong ion–lattice coupling via the JT effect.

4.1. The one-electron model

A review of the theory of deep level impurities in semiconductors has been given by Zunger (1986). In this approach, the Coulomb interactions between the localised (open

shell) electrons are added to the calculated mean-field one-electron energies. This predicts that, for Cr^{3+} ions in GaAs, the ground state is $^4T_1$, derived from the e^2t_2 one-electron configuration, but that close to it is another ^2E state derived from the e^3 configuration. Above this is a $^2T_1$ state. From these calculations, it appears that the $^4T_1$–^2E gap is quite small. In fact, for the isoelectronic V^{2+} ion in GaAs, it has been predicted that the ground state is ^2E and not $^4T_1$ (Katayama-Yoshida and Zunger 1986, Caldas *et al* 1986). This has been supported by phonon scattering experiments (Butler *et al* 1987, 1989, Sahraoui-Tahar *et al* 1989) and also by optically detected EPR experiments (Gorger *et al* 1988).

The $^4T_1$ ground state is coupled to the ^2E state (and also to the $^2T_1$ state) by spin–orbit coupling. As the $^4T_1$–^2E gap is small, sizeable admixtures of ^2E within the ground state must be anticipated. The appendix describes the results of a calculation to account for this using the strong-field method of Sugano *et al* (1970). The result, including also the coupling to the $^2T_1$ state, can be described by an effective Hamiltonian for the $^4T_1$ ground state in terms of an effective orbital operator $l = 1$ and a real spin $S = \frac{3}{2}$. This Hamiltonian is

$$\mathcal{H}_{\text{eff}} = A(\boldsymbol{l}\cdot\boldsymbol{S}) + B(\boldsymbol{l}\cdot\boldsymbol{S})^2 + C(E^l_\theta E^s_\theta + E^l_\varepsilon E^s_\varepsilon) + El(l+1)S(S+1) \tag{4.1}$$

where E^l_θ and E^l_ε are the orbital operators

$$E^l_\theta = \tfrac{1}{2}[3l_z^2 - l(l+1)] \qquad E^l_\varepsilon = \tfrac{1}{4}\sqrt{3}(l_+^2 + l_-^2) \tag{4.2}$$

and E^s_θ is equivalent to E^l_θ with l replaced by S. The z axis is defined to lie along the [001] direction. The parameters A, B and C are given by

$$\begin{aligned} A = a' &= -\tfrac{1}{6}(\xi'^2/E + \xi^2/T) & C = c' &= -\tfrac{2}{3}(\xi'^2/E) \\ B = b' &= \tfrac{1}{9}(3\xi'^2/E + \xi^2/T) & E = e' &= -\tfrac{1}{2}(3\xi'^2/E + \xi^2/T) \end{aligned} \tag{4.3}$$

where ξ' and ξ are the off-diagonal and diagonal one-electron spin–orbit coupling parameters respectively as defined in (A3) and E and T are the energies of ^2E and $^2T_1$ relative to $^4T_1$ respectively.

4.2. The Jahn–Teller effect

The experimental data summarised earlier strongly suggests the following basic properties of the Cr^{3+} ion:

(i) the ion is strongly coupled to both e- and t_2-type displacements;

(ii) the ground states must be constructed from states localised in the orthorhombic wells;

(iii) strain plays a vital rôle in characterising the EPR spectrum.

There are several approaches to this problem as described, for example, by Bersuker and Polinger (1989). However, it is most convenient here to use the ideas and notation defined in the unitary transformation method developed by two of the present authors (Bates *et al* 1987, Dunn 1988, Dunn and Bates 1989a). This approach is particularly appropriate here because the second-order JT reduction factors for orthorhombic systems have only been calculated by this method (Dunn and Bates 1989b).

The ground states of the vibronic Hamiltonian for a $T_1 \otimes (e + t_2)$ JT system consist of a T_1 vibronic triplet with an excited T_2 vibronic triplet at a relative energy δ (Dunn and Bates 1989a, equation (4.3)). The vibronic triplets are both split and coupled by the

spin–orbit coupling. Provided δ is sufficiently large, the effect of the spin–orbit coupling within each triplet can again be described by the effective Hamiltonian (4.1) where, for the $^4T_1$ vibronic ground state (Dunn and Bates 1989b),

$$\begin{aligned} A &= a'' = K_{11}^{et}(T_1)k_1(T_1)\lambda - 2F_1k_1(T_1)^2 \\ B &= b'' = [-2(F_1 + 4F_3 + 2F_4 + F_5) + G]k_1(T_1)^2 \\ C &= c'' = [\tfrac{2}{5}(5F_1 - 2F_2 + 4F_3 - F_5) - \tfrac{4}{3}G]k_1(T_1)^2 \\ E &= e'' = (\tfrac{1}{2}c'' - 2F_1)k_1(T_1)^2 \end{aligned} \tag{4.4}$$

and where $K_{11}^{et}(T_1)$ is the first-order JT reduction factor for orbital operators of T_1 symmetry, F_1–F_5 are second-order JT reduction factors defined by

$$F_n = \lambda^2 f_n^{et} N_{T1et}^2$$

and G allows for coupling between the T_1 and T_2 ground states such that $G = \lambda^2 g_n^{et}$ where f_n^{et} and g^{et} are defined in Dunn and Bates (1989b), equations (4.13) and (4.14). $k_1(T_1)$ is the isomorphic constant.

4.3. *The effective Hamiltonian*

The total effective Hamiltonian is obtained by adding to (4.4) a part to allow for $^2E(^2T_1)$–$^4T_1$ mixing corrected for JT effects. As the ion–lattice interaction Hamiltonian has zero matrix elements between the two states, it is sufficient to incorporate the JT effect into the parameters given in (4.3) by the addition of first-order reduction factors. This is readily accomplished for the first and third terms by multiplying them by $K_{11}^{et}(T_1)$ and $K_{11}^{et}(E)$ respectively (the symbol in brackets gives the symmetry of the orbital operator involved). However, it is necesary to rewrite the second term as a sum of symmetry-adapted operators and then insert the appropriate reduction factors. After a little manipulation, the result can be rewritten in the form of (4.1) where, neglecting the constant term,

$$\begin{aligned} A &= a_0 = \tfrac{1}{2}b'K_{11}^{et}(T_2) + (a' - \tfrac{1}{2}b')K_{11}^{et}(T_1) \\ B &= b_0 = \tfrac{1}{2}b'K_{11}^{et}(T_2) \\ C &= c_0 = c'K_{11}^{et}(E) + \tfrac{2}{3}b'(K_{11}^{et}(E) - K_{11}^{et}(T_2)). \end{aligned} \tag{4.5}$$

Combining (4.5) with (4.4) the effective Hamiltonian (4.1) can again be used with

$$A = a = a_0 + a'' \qquad B = b = b_0 + b'' \qquad C = c = c_0 + c''. \tag{4.6}$$

In the presence of a magnetic field $\boldsymbol{B}$, the additional Hamiltonian is given by

$$\begin{aligned} \mathcal{H}_{\boldsymbol{B}} = \mu_B\{&(g_e + f)(\boldsymbol{B}\cdot\boldsymbol{S}) + d(\boldsymbol{l}\cdot\boldsymbol{B}) + e[(\boldsymbol{l}\cdot\boldsymbol{S})(\boldsymbol{l}\cdot\boldsymbol{B}) + (\boldsymbol{l}\cdot\boldsymbol{B})(\boldsymbol{l}\cdot\boldsymbol{S})] \\ &+ f(E_\theta^l E_\theta^{SB} + E_\varepsilon^l E_\varepsilon^{SB})\} \end{aligned} \tag{4.7}$$

where $E_\theta^{SB} = \frac{1}{2}(3B_zS_z - \boldsymbol{B}\cdot\boldsymbol{S})$ etc, $g_l = 2.0023$, and d, e and f are the parameters involving the first- and second-order JT reduction factors respectively such that

$$d = k_1(T_1)K_{11}^{et}(T_1) \qquad e = b''/\lambda \qquad f = 2c''/\lambda. \tag{4.8}$$

Table 1. Definitions of the orthorhombic sites, labelled by k. The notation used by KS and SK are also given for comparison.

Direction of well	Ground orbital state	Labels		
		k	SK	KS
[110]	$\sqrt{\frac{1}{2}}(x+y)$	1	5	6
[1$\bar{1}$0]	$\sqrt{\frac{1}{2}}(x-y)$	2	6	5
[011]	$\sqrt{\frac{1}{2}}(y+z)$	3	1	1
[01$\bar{1}$]	$\sqrt{\frac{1}{2}}(y-z)$	4	2	2
[101]	$\sqrt{\frac{1}{2}}(z+x)$	5	3	3
[$\bar{1}$01]	$\sqrt{\frac{1}{2}}(z-x)$	6	4	4

5. The model for the EPR spectra

In a real crystal, there will be a distribution of ions at sites with different strains, so the corresponding EPR peaks occur at different magnetic fields. Thus the EPR spectrum consists of a composite of resonances from sites at all strains. In the present example, the dominant part of the strain is caused by the sample mounting. As the spectra show orthorhombic ⟨110⟩ symmetry, it is clear that such sites dominate the observed spectrum and that in strain-free crystals no resonances are observed. The largest peaks in intensity will be observed from sites that are orthorhombically strain-stabilised, in which resonances from sites with different strain magnitudes occur at the same magnetic field. This situation occurs when the relative separation of two energy levels remains constant over a large range of strains. Strain-stabilised resonances have been identified previously for the GaAs:Cr^{2+} (Abhvani *et al* 1982, 1984), GaP:Cr^{2+}(Ib) (Bates *et al* 1984) and GaP:Cr^{3+} (Dunn *et al* 1986) systems. However, GaAs:Cr^{3+} is probably the best example of strain stabilisation as the spectra display all the expected orthorhombic properties.

As a direct consequence of this orthorhombic symmetry and of the strong coupling of the ion to its surroundings, the JT effect for the ion must be of $T \otimes (e + t_2)$ type. The two vibronic triplets T_1 and T_2 present in a strain-free situation are each split by the orthorhombic strain into three singlets (Dunn and Bates 1988, figure 2). An alternative description in the very strong coupling limit is to suppose that for a particular ion, the [110] strain lowers the energy of the well labelled '1' by more than that of any other well. The system retains this static distortion for all time unless disturbed by other perturbations. Table 1 defines the labels k for the six orthorhombic wells to be used throughout this paper in terms of the cubic axes and the orbital ground states. The corresponding notations for the sites used by KS and SK are also given in the table.

In addition to splitting the vibronic triplets, the strain will also couple them together. However, provided δ is sufficiently large compared with the magnitude of the strain, the two triplets will nevertheless remain separate. The ground states will all belong to the T_1 triplet and thus the existence of the levels derived from the T_2 triplet can be forgotten as far as the EPR spectrum is concerned. We will make this assumption here. Another effect of the strain is to shift the wells in Q-space by a small amount. This in turn could be expected to alter the reduction factors defined for the unstrained system. However, this shift is very small and detailed calculations verify that the changes in the reduction factors can be neglected.

Considering the T_1 vibronic states only, the Hamiltonian representing a [110] strain (which lowers the [110] well) is

$$\mathcal{H}_{\text{strain}} = -\tfrac{1}{2}\bar{V}_E\bar{Q}_\theta E^l_\theta + \tfrac{3}{2}\bar{V}_T\bar{Q}_6 T_{xy} \tag{5.1}$$

and where $\bar{V}_E$ and $\bar{V}_T$ are equivalent to V_E and V_T respectively multiplied by the appropriate reduction factors, and $\bar{Q}_\theta$ and $\bar{Q}_6$ are the static contributions to Q_θ and Q_6 of strains of E_θ and T_{xy} symmetry respectively. It is preferable here to rewrite $\mathcal{H}_{\text{strain}}$ in the form

$$\mathcal{H}_{\text{strain}} = V(\sin\gamma E_\theta + \cos\gamma T_{xy}) \tag{5.2}$$

where $V = \frac{1}{2}[(\bar{V}_E\bar{Q}_E)^2 + 9(\bar{V}_T\bar{Q}_6)^2]^{1/2}$ and $\tan\gamma = -3\bar{V}_T\bar{Q}_6/\bar{V}_E\bar{Q}_E$. The parameter γ is unique for a particular system; it determines the direction in the five-dimensional Q-space along which the pure orthorhombic sites of C_{2v} symmetry exist. This is in contrast to the $T \otimes e$ and $T \otimes t_2$ systems for each of which the directions in Q-space along which the tetragonal and trigonal sites respectively occur is the same for all systems.

Provided V is large enough and of the correct sign, equation (5.2) describes the states that give the strain-stabilised spectra. Values for the parameters cannot be deduced reliably by calculation as many contributions occur. Instead they will be obtained by fitting the EPR data of KS and our own TD EPR data.

6. Results

KS showed that their EPR spectra arose from transitions between the Zeeman components of the ground and first excited doublets. It is necessary to identify such levels from the Hamiltonian

$$\mathcal{H} = \mathcal{H}_{\text{eff}} + \mathcal{H}_B + \mathcal{H}_{\text{strain}} \tag{6.1}$$

and at the same time involve the symmetry-related sites in order to give a complete description of the isofrequency curves ($\mathcal{H}_{\text{eff}}$ has the parameters given by (4.6)).

Programs have been devised to obtain values for the parameters a, b, c, d, e, f and γ in the strain-stabilised region. The experimental data were made up of:

(i) the EPR data of KS given in their figure 3 and table 1 (and reproduced in figure 5);
(ii) the TD EPR data given here in figure 4;
(iii) a few points from the TD EPR data isofrequency curves at 8.7 GHz (figure 2).

The most difficult task was to relate the various peaks in the spectra with the site and to correlate these with the signs of both V and γ. V was taken to be negative and with a magnitude large enough to satisfy the strain-stabilisation condition. It was found that the fitting procedure was particularly sensitive to the parameters a and γ. Taking a positive, a good fit was found with

$$\begin{aligned} a &= (6.55 \pm 0.3)\ \text{cm}^{-1} & d &= (1.6 \pm 0.4) \times 10^{-2}\ \text{cm}^{-1} \\ b &= -(2.05 \pm 0.3) \times 10^{-1}\ \text{cm}^{-1} & e &= (3.5 \pm 1.0) \times 10^{-4}\ \text{cm}^{-1} \\ c &= -(8 \pm 3) \times 10^{-2}\ \text{cm}^{-1} & f &= (1.35 \pm 0.3) \times 10^{-3}\ \text{cm}^{-1}. \end{aligned} \tag{6.2}$$

and $\gamma = 1.23 \pm 0.01$ with $V = -45\ \text{cm}^{-1}$.

With this set of parameters, all the calculated values for B_{res} were within the relevant experimental uncertainty (which varied markedly between the different data points).

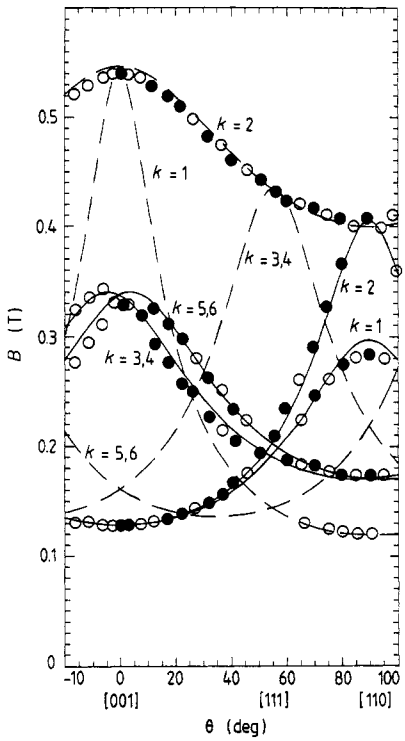

Figure 5. The calculated isofrequency curves for $\nu = 9.1614$ GHz for $\boldsymbol{B}$ in the $(1\bar{1}0)$ plane and the experimental points of KS (● and ○). The points indicated thus ● were included in the fitting routine. Full curves refer to transitions within the lower doublet and the broken curves to the upper doublet. The site is also labelled by the k-value.

The tolerances quoted in the above parameter values were those for which the increase in F was less than ~1%. It was clear that F was sensitive to changes in γ and, to a lesser extent, in a. However, the parameters d, e and f (the second-order corrections to the Zeeman terms) produced only small changes in F. In fact, putting $d = e = f = 0$ increased F by a factor of less than 2 and the fit was only marginally worse for a few of the data points.

Detailed investigations have shown that the resonances within the lower doublet were strain-stabilised for $V \simeq -20\,\text{cm}^{-1}$ but, within the upper doublet, a value of $\simeq -40\,\text{cm}^{-1}$ was needed for strain stabilisation. This implies that many more sites contribute to the strain-stabilised spectrum for the lower doublet compared to the upper doublet. Consequently the relative intensities of the two types of transition will vary with the sample and the details of the mounting of the sample as found experimentally.

Figure 5 shows the experimental points of KS together with the calculated isofrequency curves for $\boldsymbol{B}$ in the $(1\bar{1}0)$ plane for the above fit with $\nu = 9.155$ GHz. (The points used in the fitting routine are indicated in the figure.) Similarly, figure 4 shows the calculated TD EPR $\boldsymbol{B}$ versus ν curves together with the experimental points. An independent check on the quality of the fit is illustrated in figures 2 and 3 which show both the experimental TD EPR points and the calculated isofrequency curves for $\nu = 8.7$ GHz for $\boldsymbol{B}$ in the (001) plane and for $\nu = 8.83$ GHz for $\boldsymbol{B}$ in the (110) plane. It is clear that the calculated curves lie well within the experimental uncertainties.

A further analysis was undertaken in which a was restricted to negative values only. A second set of parameters were found that gave an acceptable fit to the transitions within the ground doublet only for all the relevant sites. However, this set was not such

a good fit as that given above and, as it did *not* fit any of the transitions within the upper doublet, we discount this set of parameter values.

7. Analysis of the results and discussion

7.1. The energy level structure and the EPR *spectrum*

The set of parameters (6.2) gives the splitting $2Q$ between the zero-field ground doublets as $3.9 \pm 0.1\ cm^{-1}$. The other doublets belonging to T_1 have relative energies of the order of 30, 35, 83 (twice) cm^{-1} for $V = -45\ cm^{-1}$. The value deduced for $2Q$ is very close to the first value ($5\ cm^{-1}$) quoted by KS. The second estimate of $2Q$ made by KS from their temperature-dependent measurements is inevitably inaccurate as other levels should have been included in their analysis. However, a much larger correction factor should have been incorporated to reflect the differences in the number of sites contributing to the strain-stabilised spectra for the two types of transition.

The parameters (6.2) have also been used to predict the energy level scheme for the Cr^{3+} ion in a strain-free environment. The ground state is a $J = \frac{1}{2}$ doublet; the $J = \frac{3}{2}$ states have a relative energy of about $11\ cm^{-1}$ and the $J = \frac{5}{2}$ states an energy of approximately $27\ cm^{-1}$. The inversion splitting δ is about $23\ cm^{-1}$ (section 2.1) so the spread in energies of the spin–orbit-split levels from the T_1 and T_2 vibronic states overlap with each other only slightly. The neglect of the T_2 vibronic levels above is thus a reasonable approximation.

For sites at zero strain and a quantum of 8.83 GHz, the isofrequency curve is virtually isotropic at a field of 0.196 T for transitions within the ground doublet. The corresponding curves for the upper doublet have fields that vary between 0.397 and 0.405 T. This upper resonance occurs at a field that is slightly higher than that found from strain-stabilised sites for $\boldsymbol{B}$ along [110]. SK note that small [110] uniaxial stresses shift this resonance to slightly lower fields, in agreement with our calculations. The other relatively strong resonance is at a field of about 0.287 T. The zero-strain resonance is predicted to be at a lower field and, although it is not so clear, the calculations again are in agreement with the experiments.

In principle, it is possible to use the results (6.2) together with the 12×12 matrix of $\mathcal{H}_{\text{eff}}$ to project out the spin Hamiltonian (3.1) for the two lowest doublets alone. The parameters D and E and the g-values could then be deduced involving λ, ξ and ξ'. However, such a calculation is very lengthy and serves little purpose as many approximations are necessarily introduced without any clarification of the underlying physics of the system.

7.2. Fundamental analysis

The result (6.2) together with the theoretical expressions (4.8) for the parameters should enable values for the basic JT parameters to be obtained. However, this is a complicated procedure in practice. The main difficulty is that the parameters in the effective Hamiltonian are not very reliable. In particular the errors in the Zeeman parameters d, e and f are significantly larger than the errors in the spin–orbit parameters a, b and c. Although the Zeeman parameters do not involve either of the excited ^2E or $^2T_1$ states (unlike the spin–orbit coupling parameters), the large uncertainties preclude their quantitative use.

For the remaining parameters we can make progress by assuming that the ^2E states gives much larger contributions than the $^2T_1$ states. This generates the relations

$$6.55 = A_1 + B_1\lambda \qquad -0.21 = A_2 + B_2\lambda \qquad -0.08 = A_3 + B_3\lambda \tag{7.1}$$

where

$$A_1 = \tfrac{1}{6}(K_{11}^{et}(T_2) - 2K_{11}^{et}(T_1))\mathcal{R} \qquad B_1 = -\tfrac{3}{2}(K_{11}^{et}(T_1) + 3F_1)$$

$$A_2 = \tfrac{1}{8}(K_{11}^{et}(T_2))\mathcal{R} \qquad B_2 = -\tfrac{9}{2}(2F_1 + 8F_3 - 4F_4 + 2F_5 - G)$$

$$A_3 = (2K_{11}^{et}(E) + K_{11}^{et}(T_2))\mathcal{R} \qquad B_3 = \tfrac{3}{2}(5F_1 - 2F_2 + 4F_3 - F_4 - 2G)$$

and where $\mathcal{R} = \xi'^2/E$.

Dunn and Bates (1989b) have used a cluster model to calculate both first- and second-order reduction factors as a function of the coupling parameter K_T for the $T \otimes (e + t_2)$ JT system, the bi-linear term, and the oscillator frequencies. Two values of the parameter $\eta = E_E/E_T$ where chosen. (E_E and E_T are the JT energies for the $T \otimes e$ and $T \otimes t_2$ systems respectively.) The quantities A_1 and A_2 are always positive and tend to limiting values of $\frac{1}{12}$ and $\frac{1}{8}$ respectively. A_3 is always negative with a limit of $-\frac{2}{9}$. In contrast, B_1, B_2 and B_3 are all negative and all tend to zero in the strong coupling limit. However, as the latter are multiplied by λ ($\simeq 90\ cm^{-1}$) it is necessary to know the rate at which they converge.

The importance of coupling to the ^2E state is immediately obvious, as without this coupling a would be negative. (It was noted in section 6 that the set of parameters with a negative did not fit any of the transitions associated with the upper doublet.) It is also clear that in order to satisfy the second equation for b, it is necessary that $|B_1| > 2|B_2|$, so that the positive part of b is cancelled and made slightly negative by $B_2\lambda$. Further calculations have been undertaken to determine the dependence on $K_T/\hbar\omega_T$ for $K_T/\hbar\omega_T > 2$ in order to attempt to fit (7.1). Unfortunately, whereas B_2 and B_3 involve second-order reduction factors only, B_1 involves additionally the first-order reduction factor $K_{11}^{et}(T_1)$. The calculations of the first- and second-order factors are entirely separate. It is impossible at the moment to obtain any numerical values in the required range especially as all values are also critically dependent upon the size of the bi-linear coupling term and on γ. In this region, our expressions for f_n^{et} are inaccurate because of the large number of terms involved in the summations. It is known also that our expressions for f_n^{et} are themselves only approximate. Two of the authors (CAB and JLD) are currently engaged in calculating more accurate expressions for the second-order reduction factors, using cubic combinations of the excited states within the wells, rather than the much simpler excited well states used in the original calculations (Dunn 1989). On account of these difficulties, no quantitative fit to (7.1) will be attempted here.

8. Conclusions

Our analysis of the previously reported conventional EPR results and our own TD EPR measurements has enabled us to obtain accurate values for the more important parameters appearing in the effective Hamiltonian. This is a more basic description of the Cr^{3+} ion in GaAs than that given previously by KS and SK using a spin Hamiltonian. Probably the most significant result is that the parameter a is large, probably due to its closeness to the excited ^2E state (Zunger 1986). This ensures that the spectra from

orthorhombic strain-stabilised sites give isofrequency curves having very pronounced orthorhombic symmetry. For smaller a, the spectra are likely to be much more complicated thus masking the orthorhombic features. This could explain why the GaAs : Cr^{3+} system is an ideal example in which to study the orthorhombic Jahn–Teller effect.

The problem with attempting to produce a more complete theory for this system is that no optical spectra of any sort are observed experimentally. The phonon scattering experiments provide a value for the inversion splitting δ. However, it is difficult to correlate this measurement for δ with the analysis here because there are again too many unknowns. From figure 3 of Dunn and Bates (1989b), if $\delta = 23\ \text{cm}^{-1}$ and $\hbar\omega_T = 115\ \text{cm}^{-1}$, we deduce that $E_{ET}/\hbar\omega_T$ is in the range 2.5 to 3.0, where E_{ET} is the JT energy of the $T \otimes (e + t_2)$ orthorhombic system. This gives $K_T/\hbar\omega_T = 1.5$ which would appear to be somewhat smaller than expected from our analysis but not in disagreement with it.

Acknowledgments

The authors wish to thank Professor Challis and Dr King for many discussions on this problem which has engaged us for a considerable time. Thanks are also due to Dr J Handley and Dr J L Simpson for help with some aspects of the computing. They would also like to thank the SERC and the EEC for travel grants to enable this collaboration between our two laboratories to succeed. One of us (LWP) also wishes to thank the SERC for a Research Studentship.

Appendix

In order to calculate the admixtures of excited states into the $^4T_1$ ground state via the spin–orbit coupling, it is necessary to use the strong-field coupling method as described by Sugano *et al* (1970, to be referred to as STK) and by Tanabe and Sugano (1958). The many-electron-type states of the system with m t_2 electrons and n e electrons at a T_d site must be written in the form

$$|t_2^m(S'\Gamma')\,e^n(S''\Gamma'');\, S\Gamma M_s M\rangle = |\alpha S\Gamma M_s M\rangle \tag{A1}$$

where $S = S' + S'', \ldots, |S' - S''|$, $\Gamma' \otimes \Gamma'' = \Gamma$ and where t_2 and e represent the one-electron states of T_2 and E symmetry respectively. The states (A1) combine under Russel–Saunders coupling to give terms denoted by the spin values (S', S'', S) and the irreducible representations $(\Gamma', \Gamma'', \Gamma)$ of the orbit as indicated. M_s is the total spin component and $M = 0, \pm 1$ for triplets, ± 1 for doublets and 0 for singlets.

For a spin-dependent operator such as the spin–orbit coupling, the Wigner–Eckart theorem enables us to write

$$\begin{aligned}\langle \alpha S\Gamma M_s M|\mathcal{H}_{so}|\alpha' S'\Gamma' M_s' M'\rangle = {} & (-1)^{(M_s - M_s')}[(2S+1)(\Gamma)]^{-1/2} \\ & \times \langle \alpha S\Gamma\|\mathcal{H}_{so}\|\alpha' S'\Gamma'\rangle\langle SM_s|S'M_s 1M_s - M_s'\rangle \\ & \times \langle \Gamma M|\Gamma' M'\mathrm{T}_1 M_s' - M_s\rangle \end{aligned} \tag{A2}$$

where $\langle SM_s|S'M_s' 1M_s\rangle$ is a Wigner coefficient. Also (Γ) = order of the Γ representation (1 for A, 2 for E and 3 for T_1, T_2), $\langle \alpha S\Gamma\|\mathcal{H}_{so}\|\alpha' S'\Gamma'\rangle$ is a reduced matrix element, and $\langle \Gamma M|\Gamma' M'\bar{\Gamma}\bar{M}\rangle$ a Clebsch–Gordon coefficient; these are tabulated in STK.

Table A1. Part of the matrices of the spin–orbit coupling the ground $^4T_1$ and excited $^2T_1$ and $^2T_2$ states. The parameters are defined by $L = (1/3\sqrt{2})\xi$, $L' = (1/2\sqrt{3})\xi'$. The components u, v of the orbital E state and of α, β, γ of the T_1 orbital states are defined in STK, table 3.4.

		$S'\Gamma'$	^2E				$^2T_1$					
		γ'	u		v		α		β		γ	
		M_s'	$\frac{1}{2}$	$-\frac{1}{2}$	$\frac{1}{2}$	$-\frac{1}{2}$	$\frac{1}{2}$	$-\frac{1}{2}$	$\frac{1}{2}$	$-\frac{1}{2}$	$\frac{1}{2}$	$-\frac{1}{2}$
$S\Gamma$	γ	M_s										
$^4T_1$	α	$\frac{3}{2}$	$\sqrt{3}iL'$		$-3iL'$						$\sqrt{3}L$	
		$\frac{1}{2}$		iL'		$-\sqrt{3}iL'$			$2iL$			L
		$-\frac{1}{2}$	$-iL'$		$\sqrt{3}iL'$					$2iL$	L	
		$-\frac{3}{2}$		$-\sqrt{3}iL'$		$3iL'$						$\sqrt{3}L$
	β	$\frac{3}{2}$	$\sqrt{3}L'$		$3L'$						$-\sqrt{3}iL$	
		$\frac{1}{2}$		L'		$\sqrt{3}L'$	$-2iL$					$-iL$
		$-\frac{1}{2}$	L'		$\sqrt{3}L'$						iL	
		$-\frac{3}{2}$		$\sqrt{3}L'$		$3L'$						$\sqrt{3}iL$
	γ	$\frac{3}{2}$					$-\sqrt{3}L$		$\sqrt{3}iL$			
		$\frac{1}{2}$	$4iL'$					$-L$		iL		
		$-\frac{1}{2}$		$4iL'$			$-L$		$-iL$			
		$-\frac{3}{2}$						$-\sqrt{3}L$		$-i\sqrt{3}L$		

$\mathcal{H}_{so}$ is written as a sum of one-electron spin–orbit coupling terms

$$\mathcal{H}_{so} = \sum_i \xi_i \boldsymbol{l}_i \cdot \boldsymbol{s}_i = V(^1T_1) \tag{A3}$$

in the notation of STK. The one-electron matrix elements are

$$\langle t_2 \| v(^1T_1) \| t_2 \rangle = 3i\xi \qquad \langle t_2 \| v(^1T_1) \| e \rangle = -3(2)^{1/2} i\xi' \tag{A4}$$

which serve as definitions of the one-electron diagonal and off-diagonal spin–orbit coupling constants respectively.

The procedure is now to write down the appropriate many-electron states for $^4T_1$ and ^2E and evaluate the diagonal and off-diagonal matrix elements. The results are then projected into the $^4T_1$ ground state and written as an effective Hamiltonian within the isomorphic states of $^4T_1$. (This method has been used by Brugel and Bates (1987) for calculating admixtures into the ^5E excited state of trigonal Cr^{2+} ions in GaAs from other terms.)

In addition to ^2E, admixtures of one of the $^2T_1$ states into $^4T_1$ will also be calculated. The three many-electron states are therefore

$\|t_2(^2T_2)e^2(^3A_2)^4T_1; S\Gamma M_s M\rangle$	taken as the energy zero
$\|e^3(^2E)^2E; S'\Gamma' M_s' M'\rangle$	of relative energy E
$\|t_2(^2T_2)e^2(^3A_2)^2T_1; S''\Gamma'' M_s'' M''\rangle$	of relative energy T.

From STK, Appendix VII, the reduced matrix elements required are

$$\langle ^4T_1 \| v(^1T_1) \| ^2E \rangle = i2\sqrt{6}\xi' \qquad \langle ^4T_1 \| v(^1T_1) \| ^2T_1 \rangle = i2\sqrt{2}\xi. \tag{A5}$$

where the results given in equation (A4) have been incorporated. Using the tabulated values for the Wigner and Clebsch–Gordon coefficients, the various off-diagonal matrix elements between $^4T_1$ and ^2E and between $^4T_1$ and $^2T_1$ have been calculated. The results are contained in table A1.

Using second-order perturbation theory, the admixtures of ^2E and $^2T_1$ into $^4T_1$ can be described by the effective Hamiltonian (4.1) where the parameter values, added together, are given in (4.3).

References

Abhvani A S, Austen S P, Bates C A, Parker L W and Pooler D R 1982 *J. Phys. C: Solid State Phys.* **15** 2217–31

Abhvani A S, Bates C A and Pooler D R 1984 *J. Phys. C: Solid State Phys.* **17** 1713–6

Austen S P, Bates C A and Brugel D 1984 *J. Phys. C: Solid State Phys.* **17** 1257–68

Bacci M, Montagna M, Pilla O and Viliani G 1989 *J. Phys.: Condens. Matter* **1** 1873–7

Bates C A, Darcha M, Handley J, Vasson A and Vasson A-M 1988 *Semicond. Sci. Technol.* **3** 172–7

Bates C A and Dunn J L 1989 *J. Phys.: Condens. Matter* **1** 2605–16

Bates C A, Dunn J L and Sigmund E 1987 *J. Phys. C: Solid State Phys.* **20** 1965–83 (corrigendum **20** 4015)

Bates C A, Handley J, Vasson A and Vasson A-M 1984 *J. Phys. C: Solid State Phys.* **17** L603–6

Bates C A and Stevens K W H 1986 *Rep. Prog. Phys.* **49** 783–823

Benkovskis A, Bates C A, King P J and Monk D J 1981 *B. Magn. Reson.* **2** 203

Bersuker I B and Polinger V Z 1989 *Vibronic Interactions in Molecular Crystals* (Berlin: Springer)

Brugel D and Bates C A 1987 *Semicond. Sci. Technol.* **2** 501–6

Butler N, Challis L J, Sahraoui-Tahar M, Salce B and Ulrici W 1987 *Japan J. Appl. Phys.* **26** Suppl. 675–6

—— 1989 *J. Phys: Condens. Matter* **1** 1191–203

Caldas M J, Figueirido S K and Fazzio A 1986 *Phys. Rev.* B **33** 7102–9
Challis L J, Locatelli M, Ramdane A and Salce B 1982 *J. Phys. C: Solid State Phys.* **15** 1419–32
Challis L J, Salce B, Butler N, Sahraoui-Tahar M and Ulrici W 1989 *J. Phys.: Condens. Matter* **1** 7277–93
Deveaud B, Picoli G, Lambert G and Martinez G 1984 *Phys. Rev.* B **29** 5749–62
Dunn J L 1988 *J. Phys. C: Solid State Phys.* **21** 383–399
—— 1989 *J. Phys.: Condens. Matter* **1** 7861–81
Dunn J L and Bates C A 1987 *J. Phys. C: Solid State Phys.* **20** L995–8
—— 1988 *J. Phys. C: Solid State Phys.* **21** 2495–509
—— 1989a *J. Phys.: Condens. Matter* **1** 375–94
—— 1989b *J. Phys.: Condens. Matter* **1** 2617–29
Dunn J L, Bates C A, Darcha M, Vasson A and Vasson A-M 1986 *Phys. Rev.* B **33** 2029–32
Gorger A, Meyer B K, Spaeth J-M and Hennel A M 1988 *Semicond. Sci. Technol.* **3** 832–8
Hamdache M, King P J, Murphy D T and Rampton V W 1982 *J. Phys. C: Solid State Phys.* **15** 5559–80
Katayama-Yoshida H and Zunger A 1987 *Phys. Rev.* B **33** 2961–4
Koschel W H, Bishop S G and McCombe B D 1976 *Solid State Commun.* **19** 521–4
Krebs J J and Stauss G H 1977a *Phys. Rev.* B **15** 17–22
—— 1977b *Phys. Rev.* B **16** 971–3
Ramdane A, Salce B and Challis L J 1983 *Phys. Rev.* B **27** 2554–7
Rezki M, Vasson A, Vasson A-M, Abhvani A S and Bates C A 1982 *J. Phys. C: Solid State Phys.* **15** 2207–16
Sahraoui-Tahar M, Butler N, Challis L J, Salce B and Ulrici W 1989 *Proc. 19th Conf. on Physics of Semiconductors (Polish Acad. of Sci., Warsaw)* p 1019–22
Stauss G H and Krebs J J 1980 *Phys. Rev.* B **22** 2050–9
Sugano S, Tanabe Y and Kamimura H 1970 *Multiplets of Transition Metal Ions in Crystals* (New York: Academic)
Tanabe Y and Sugano S 1958 *J. Phys. Soc. Japan* **9** 753–66
Zunger A 1986 *Solid State Physics* vol 39 (New York: Academic) pp 276–464